Available online at www.sciencedirect.com
ScienceDirect
Journal of Molecular Spectroscopy 242 (2007) 46–54
Journal of MOLECULAR SPECTROSCOPY
www.elsevier.com/locate/jms

New infrared integrated band intensities for HC_3N and extensive line list for the ν_5 and ν_6 bending modes

A. Jolly [a,*], Y. Benilan [a], A. Fayt [b]

[a] LISA, Université Paris 12, 61 Av. Général de Gaulle, F-94010 Créteil Cedex, France
[b] Laboratoire de Spectroscopie Moleculaire, Université Catholique de Louvain, Chemin du cyclotron 2, B-1348 Louvain-la-Neuve, Belgium

Received 12 December 2006; in revised form 19 January 2007
Available online 3 February 2007

Abstract

The infrared spectrum of cyanoacetylene (also called propynenitrile) has been investigated from 400 to 4000 cm^{-1} at a resolution of 0.5 cm^{-1}. Integrated intensities of the main bands and a number of weaker bands have been obtained with an uncertainty better than 5%. Inaccurate values in previous studies have been identified in particular concerning the intensity of the strong ν_5 stretching band at 663.2 cm^{-1}. Former results on the temperature dependence of integrated intensities have also been revisited.

Synthetic spectra calculation has been performed for the ν_5 and ν_6 bands on the basis of the best available high resolution data. It has been shown that the GEISA line parameters for HC_3N are not sufficient to reproduce the band intensities and some hot band features observed in our experimental spectra at room temperature. As a first step, the model spectra has been improved by including a number of missing hot subbands and by calculating accurately the hot band relative intensities. Finally, a perfect agreement between calculated and observed spectra was achieved on the basis of a global analysis of HC_3N levels up to 2000 cm^{-1} combined with the new integrated intensity measurements. A new extensive line list for the ν_5 and ν_6 bending modes of HC_3N has been compiled.

Keywords: Infrared spectra; HCCCN; Integrated intensities; Global analysis; Titan

1. Introduction

Cyanoacetylene was identified in various astrophysical objects like comets, the interstellar medium and star forming regions mainly by radio observations. By means of the two bending fundamental bands ν_5 and ν_6 at 663.2 and 498.8 cm^{-1}, HC_3N was also detected in the infrared range in Titan's atmosphere first by the Voyager mission [1,2], later by ISO [2] and very recently by the Cassini mission [3]. It has also been detected in the infrared range in an entirely different astrophysical object, the young protoplanetary nebula CRL 618 [4]. Laboratory data, and infrared spectra in particular, are rare for HC_3N. Absolute intensity measurements exist only at low resolution, and where carried out by only two teams [5–8]. Large discrepancies persist between those studies in particular concerning the intensity of ν_5, the strongest bending mode which is essential for abundance determination in planetary and astronomical environment. Also, model spectra, obtained from the available GEISA line list, are not able to reproduce our experimental spectra at 0.5 cm^{-1} resolution. This coupled experimental and theoretical work was aimed to clear out the remaining problems.

In the first section, our experimental results are presented and compared to the previous studies with an emphasis on saturation effects. Then we discuss the temperature dependence of absorption measurements which is important to interpret spectra obtained in cold regions like Titan's atmosphere. The crucial role of hot subband intensities for molecules with low lying vibrational levels is then examined, in particular the difficulties in simulating low resolution band spectra using data from high resolution experiments. We compare our experimental spectra with

* Corresponding author. Fax: +33 1 45171564.
E-mail address: jolly@lisa.univ-paris12.fr (A. Jolly).

0022-2852/$ - see front matter © 2007 Published by Elsevier Inc.
doi:10.1016/j.jms.2007.01.008

a model spectra using the GEISA line parameters and propose improvements to obtain a better fit. Finally we briefly present the global rovibrational analysis we have used to obtain a perfect fit to our experimental spectra and propose a new complete line list for the ν_5 and ν_6 bending modes of HC_3N. Model spectra are then calculated at 200 K in order to test the possibility to detect HC_3N hot subbands on Titan.

2. Experimental results

Uyemura's team has first obtained the integrated intensities for the stretching fundamental of cyanoacetylene [5] and later for the very important bending modes ν_5, ν_6 and ν_7 [6]. Those studies were conducted at 1.6 cm^{-1} resolution and 273 K. Khlifi and colleagues have studied the intensity of most of the bands except the low lying (223 cm^{-1}) weak bending mode ν_7 [7]. The resolution was 4.0 cm^{-1} and the temperature 308 K according to the authors. Later, they measured the intensity of ν_1, ν_2, ν_5 and ν_6 versus temperature between 225 and 325 K [8].

In our experiment, a 25 cm long multipass cell was used to measure absorption spectra of HC_3N at room temperature (296 K) using a Bruker Equinox 55 FTIR spectrometer at 0.5 cm^{-1} resolution. We use a KBr beamsplitter and a DTGS D301 detector which has a linear response from 400 to 5000 cm^{-1}. The optical path was set to 105 cm and the pressure ranged from 0.033 to 22.3 mbar. For each pressure, spectra of the pure sample and of the mixture of this sample with about 1000 mbar nitrogen were recorded in order to control the saturation effects. Hundred scans have been recorded and coadded for each spectrum. Fig. 1 presents the experimental absorption coefficient for the two strong bending modes ν_5 and ν_6, and also for the $(\nu_6 + \nu_7)$ combination band. Our results are presented in two separate tables. Table 1 presents all the results of our work concerning the fundamental modes compared to the previous studies. Our values and uncertainties are derived for each band from the average and the standard deviation of the measured integrated band coefficients from spectra which did not suffer from saturation. Our uncertainties did nod not exceed 5% for the fundamental bands. The agreement with Uyemura's results is very good, in particular for the important ν_5 band intensity which seems to confirm this value and rule out the much lower value obtained by Khlifi in 1990. As we will show below, saturation problems can explain the discrepancies with Khlifi's results. Table 2 presents the intensities obtained for combination and overtone bands measured at very high column density. All those results can also be found in our spectroscopic data base at the following internet link: http://www.lisa.univ-paris12.fr/GPCOS/SCOOPweb/SCOOP.html.

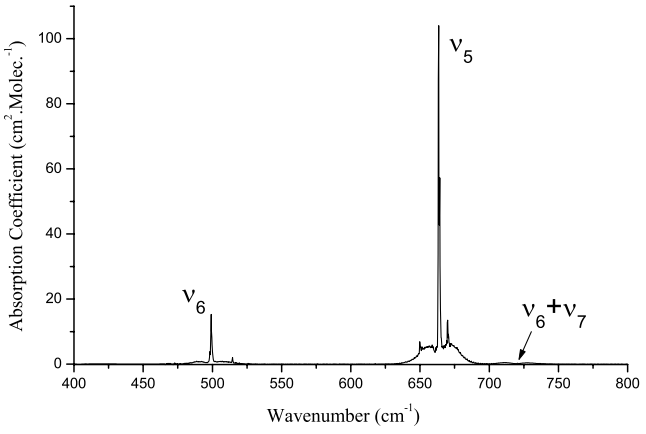

Fig. 1. Infrared absorption coefficient of HC_3N at 0.5 cm^{-1} resolution and 296 K in the bending region.

Most experimentalists take advantage of the pressure broadening, induced by inert gas like molecular nitrogen, to avoid the saturation effects which prevent from measuring absolute integrated intensities in low resolution absorption measurements. The linearity of the integrated intensities versus sample pressure is verified by Beers' law plots to ensure that no saturation is occurring. Both Uyemura and Khlifi, in their respective papers [6,7], show Beer's law plots which are perfectly linear. But looking more carefully, an important difference appears concerning the column density range of both studies. For ν_5, the strongest bending mode of HC_3N, the last point on Uyemura's plot is obtained for 9 mbar and a 5 cm path length

Table 1
Position and absolute intensity of the fundamental vibrational modes of HC_3N

Mode	Vibration	Position (cm^{-1})	Absolute intensity (cm^{-2} atm^{-1})			
			This work	Uyemura[a](1974, 1982)	Khlifi[b] (1990)	Khlifi[c] (1992)
ν_1	CH str.	3327	249.4 ± 12	248.7 ± 37	285 ± 15	253–215
ν_2	CC str.	2274	40.7 ± 2.2	40.8 ± 6.1	39.8 ± 1.1	39–32
ν_3	CN str.	2079	8.0 ± 1.0	7.8 ± 1.2	8.8 ± 0.3	—
ν_4	CC str.	862	0.68 ± 0.03	—	0.8 ± 0.1	—
ν_5	CH bend.	663.2	268.6 ± 7.0	281 ± 41	207 ± 9	224–249
ν_6	CN bend.	498.8	39.0 ± 1.9	32.9 ± 5.0	32.1 ± 1.7	37–52
ν_7	CC bend.	222.4	—	0.73 ± 0.11	—	—

[a] Converted from km/mol to cm^{-2} atm^{-1}.
[b] Converted from $T = 308$ K to $T = 296$ K.
[c] Reported values correspond to measurements at 225 and 325 K, respectively.

Table 2
Position and absolute intensity of harmonic and combination bands of HC_3N

Band	Position (cm^{-1})	Absolute intensity ($cm^{-2}\,atm^{-1}$)	
		This work	Khlifi (1990)[a]
$\nu_1+\nu_7$	3549	1.47 ± 0.07	
$\nu_2+\nu_4$	3133	2.6 ± 0.25	
$\nu_1-\nu_7$	3104		
$\nu_2+\nu_6$	2766	1.25 ± 0.15	
$\nu_1-\nu_5$	2665	0.52 ± 0.04	
$\nu_3+\nu_6$	2575	0.71 ± 0.04	
$\nu_2+\nu_7$	2494	1.38 ± 0.07	
$3\nu_5$	1970	0.09 ± 0.02	
$2\nu_5$	1314	70.5 ± 3.5	69.5 ± 1.8
$\nu_5+\nu_6$	1163	0.11 ± 0.02	
$\nu_4+\nu_7$	1090	0.32 ± 0.05	
$2\nu_6$	1013	1.72 ± 0.21	2.2 ± 0.7
$\nu_6+\nu_7$	720.3	12.1 ± 0.9	12.1 ± 0.7

[a] Converted from $T = 308$ K to $T = 296$ K.

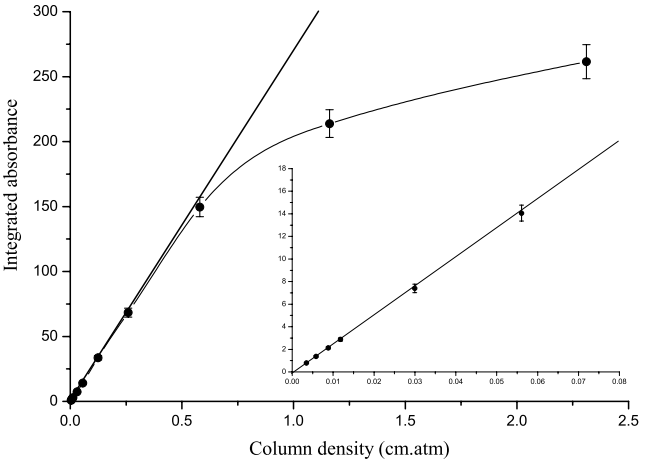

Fig. 3. Saturation curve of the ν_1 band of HC_3N for column densities up to 2.5 cm atm with zoom section up to 0.08 cm atm.

(0.045 cm atm) while Khlifi's last point is at 53 mbar with a 10 cm path length (0.53 cm atm).

In this new study, we have used very low (0.0033 cm atm) and very high (2.23 cm atm) column densities to show that non-linearity does appear even with 1 atm of nitrogen added to the sample. Fig. 2 shows the saturation curve for the ν_5 band obtained from our measurements at 10 different pressures. The non-linearity appears for column densities higher than 0.10 cm atm, with differences of 4%, 18%, and 40% at 0.12, 0.25, and 0.58 cm atm, respectively. Uyemura's measurements which did not exceed a column density of 0.045 cm atm are well in the linear zone. This is obviously not the case for Khlifi's last measurement which was obtained at 0.53 cm atm. Our result for the band intensity of ν_5 obtained from an average of the measurements obtained in the linear zone is 268 $cm^{-2}\,atm^{-1}$ in good agreement with Uyemura's value of 281 $cm^{-2}\,atm^{-1}$ [6] taking into account the uncertainties. The value measured by Khlifi, 207 $cm^{-2}\,atm^{-1}$, should rise to about 275 $cm^{-2}\,atm^{-1}$ if the saturation effect was taken into account.

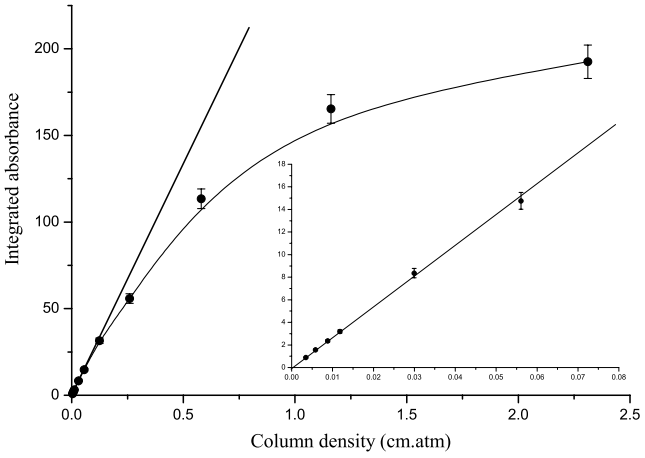

Fig. 2. Saturation curve for the ν_5 band of HC_3N up to 2.5 cm atm and zoom section up to 0.08 cm atm.

Saturation effects strongly depend on the shape of the band and this is visible when comparing the behavior of two bands which have about the same integrated intensity but very different shapes, the parallel ν_1 band without Q branch and the perpendicular ν_5 band with its sharp Q branch. Fig. 3 shows that saturation does not occur for ν_1 before about 0.5 cm atm so that Khlifi was able to obtain a non-saturated value for this band. Our result for the band intensity of ν_1 is 249 $cm^{-2}\,atm^{-1}$, in very good agreement with Uyemura's value of 248 $cm^{-2}\,atm^{-1}$. Khlifi's value is about 15% higher at 285 $cm^{-2}\,atm^{-1}$ but saturation effects cannot explain this difference.

The resolution of the instruments can also play a role in the saturation evoked here, but the resolution of all experimental works discussed here is comparable, and the small difference should not play an important role. In fact, the worst resolution (4 cm^{-1}) of all three experiments concerns Khlifi's work, what means that the saturation could be slightly stronger than for Uyemura and our work.

For ν_6, we found a value of 39.0 $cm^{-2}\,atm^{-1}$ which is higher than the previous measurements by Uyemura who found 32.9 $cm^{-2}\,atm^{-1}$ and Khlifi 32.1 $cm^{-2}\,atm^{-1}$. Saturation problems should not occur for such a weak transition and cannot explain the present discrepancy. The results from Khlifi's second paper [8] are also listed in Table 1. Some results are surprisingly different compared to the first paper. In this second paper the temperature has been adjusted between 225 and 325 K, and the integrated intensity for the ν_6 band spreads from 37 to 52 $cm^{-2}\,atm^{-1}$ and is equal to 44.5 $cm^{-2}\,atm^{-1}$ at 296 K. This is not coherent with the previously measured value of 32.1 $cm^{-2}\,atm^{-1}$ reported in the first paper but is closer to our own measurements.

In conclusion, we have confirmed the results obtained by Uyemura and we have shown that some discrepancies in the Khlifi's results can be explained by saturation effects.

3. Temperature dependence

The temperature dependence of absorption intensities is an important issue since very different temperature conditions are found in the astronomical environment. In particular, the temperature range sounded by infrared observations of Titan's atmosphere is about 100–200 K which is much colder than the conditions in most laboratory studies. Therefore, the temperature dependence is essential to compare laboratory results obtained in different temperature conditions. Few experiments report absolute absorption intensities versus temperature, only one for HC_3N, the second paper by Khlifi [8]. The authors observe a variation of the band intensities smaller than 20% over the 225–325 K range. With increasing temperature, a slight decrease of the intensity is observed in most bands but surprisingly a small increase of 5% is observed for the ν_5 band. Those results are questionable since the uncertainty of the experimental values should be higher than 10% on the basis of the important dispersion of the tabulated values reported by the authors.

Theoretically, the vibrational band intensity can be expressed as

$$S_V^0 = \frac{8\pi^3}{3hc}\nu_0\, N|\langle\mu_{vib}\rangle|^2 \frac{g_{vib}}{Q_{vib}} e^{-hc\nu_0/kT} \quad (1)$$

where ν_0 is the band origin, $|\langle\mu_{vib}\rangle|$ is the vibrational transition dipole moment, g_{vib} the vibrational degeneracy and N denotes the total number of absorbing molecules per cm^3 at a standard pressure of 1 atm: $N = L * 273.15/T$ where L is the number of molecules per cm^3 at a pressure of 1 atm and at 0 °C. The exponential term in relation (1) is the Boltzmann factor and gives the population of the lower level of the transition. This term together with the vibrational partition function Q_{vib} is responsible for the temperature dependence of the band intensity. Relation (1) is accurate for one single vibrational band but at low resolution the integration corresponds to the whole band system including all hot bands. Thus, low resolution integrated intensity measurements should be compared to the sum over all populated vibrational states:

$$S_V^{BS} = \sum_{vib} S_V^0 \quad (2)$$

The vibrational dipole moment can be considered as equal for all bands of the same band system. Furthermore, we can use the relation of the vibrational partition function and finally, by calculating the various constants, using $L = 2.687\ 10^{-19}\ atm^{-1}\ cm^{-3}$, with the dipole moment in Debye and ν_0 in cm^{-1}, we obtain:

$$S_V^{BS} = 11.1858\nu_0 \frac{273.15}{T}|\langle\mu_{vib}\rangle|^2 \quad (3)$$

which means that the temperature dependence of low resolution integrated band intensity measurement should be $1/T$, what expresses only the fact that the number of absorbing molecules per cm^3 at a fixed pressure varies with $1/T$.

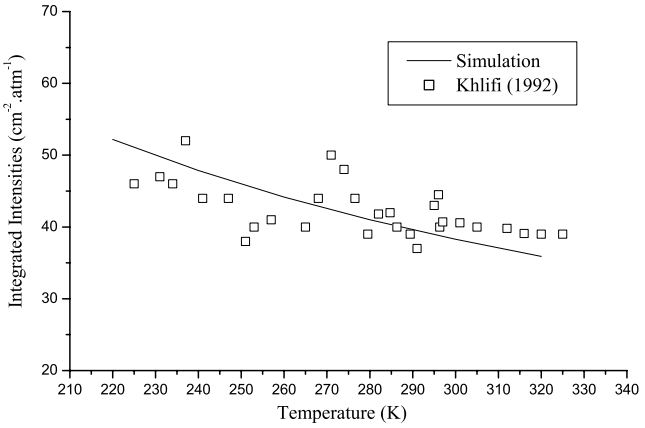

Fig. 4. Khlifi's et al. [8] experimental values for the ν_6 band intensities compared to the $1/T$ model using the value obtained in this work at 296 K ($39.0\ cm^{-2}\ atm^{-1}$).

Instead of this simple formulation, Khlifi proposed to match his measured intensity values with an empirical formulation including an extra term $(T/T_0)^{\beta}$ where β is determined for each band using the experimental data. Khlifi's result is quite surprising since the value of β appears to be very different for the four studied bands ranging from 0.25 for ν_2 to 1.25 for ν_5. In fact, as can be seen in Fig. 4, the simple $1/T$ model fits reasonably well Khlifi's ν_6 data and it does not seem necessary to resort to a more complicated model which has no theoretical background. The small increase (5%) observed by Khlifi for the ν_5 band can of course not be reproduced by the $1/T$ model. In fact, the behavior of this band is exactly what is expected for a saturated band, a stagnation of the measured intensity. As seen previously, saturation of the ν_5 band was proved to have occurred in Khlifi's first paper and could be also responsible for the inaccurate results on the temperature dependence of this band.

In conclusion, Khlifi's empirical formulation does not seem to be adequate and should not be used for extrapolation of band intensities to low temperature. Instead, the $1/T$ formulation which is theoretically established is recommended as long as no experimental work can disprove it.

4. Band spectra simulation

Line positions and line intensities proposed by the GEISA database allow line by line simulation and so are essential for the interpretation of observed spectra. However, for HC_3N and all molecules with low lying vibrational modes, line intensities and integrated band intensities must be taken with care because of the important role played by hot subbands.

The first high resolution ($0.04\ cm^{-1}$) infrared study of cyanoacetylene concerned the two bending modes ν_5 and ν_6 [9]. The authors have obtained the band origin and the rotational constants of the upper states for both bands by fixing the ground state constants according to the microwave spectra [10,11]. Strong hot subbands have been

identified for both modes but an assignment was proposed only for v_6. Later, Arié and colleagues [12] have investigated the same region with a resolution of 0.002 cm^{-1} and have obtained the rotational parameters for the fundamental v_5 transition and 12 associated hot subbands, with *e* and *f* components counted separately. The fundamental transition v_6 was also analyzed, with 7 hot subbands. None of the high resolution studies included intensity measurements. The data found in the GEISA data base are based on Arié's experimental work for the line positions and the assignment of all hot bands. As mentioned by Arié, the intensities have also been computed and included in the GEISA database. No details are given about this computation, but it appears that the values of Khlifi's first low resolution work [7] have been used.

To find out, we have calculated the sum of the intensities of the lines belonging to the fundamental band v_6 in GEISA. We have found a total intensity of 14.3 $cm^{-2}\,atm^{-1}$ which corresponds to a total integrated intensity of the band equal to 43.2 $cm^{-2}\,atm^{-1}$ taking into account the vibrational partition function $Q_v = 3.03$ for HC_3N at 296 K. This integrated intensity value for the v_6 band corresponds to the result at 296 K from the temperature dependent work by Khlifi [8] which is almost 50% higher than the previously published values of 32.9 $cm^{-2}\,atm^{-1}$ by Uyemura [6] and 32.1 $cm^{-2}\,atm^{-1}$ by Khlifi et al. in the first paper [7].

GEISA also includes the lines from the hot bands analyzed in Arié's high resolution work [12]. For the v_6 band system, four hot subbands from v_7 (223 cm^{-1}) and three hot subbands from v_6 (499 cm^{-1}) have been assigned. The integrated intensities of those hot transitions can also be obtained by summing the intensities of the selected lines. The sum for the $v_6 + v_7 \leftarrow v_7$ hot subbands is 9.7 $cm^{-2}\,atm^{-1}$ equally shared by the 4 subbands ($\Sigma^+ \leftarrow \Pi$, $\Sigma^- \leftarrow \Pi$ and two $\Delta \leftarrow \Pi$), and 2.5 $cm^{-2}\,atm^{-1}$ for the other 3 subbands ($2v_6 \leftarrow v_6$) where the subband of type $\Sigma \leftarrow \Pi$ has the same intensity as the two $\Delta \leftarrow \Pi$ subbands together. The integrated intensities of the hot bands found in GEISA can be calculated from the Boltzman factor multiplied by 2. As we will see below, the way hot subband intensities have been calculated is not correct. The sum of all the subbands included in GEISA for v_6 is thus 26.6 $cm^{-2}\,atm^{-1}$ which is 40% lower then the original total band intensity of 43.2 $cm^{-2}\,atm^{-1}$. This is easily understandable since many hot subbands with non-negligible intensity have not been analyzed and thus not included in the database. For example, hot subbands with lower states $2v_7$(446 cm^{-1}) and v_5 (663 cm^{-1}) are not taken into account.

For the v_5 band, 12 subbands with lower states v_7 (223 cm^{-1}), $2v_7$ (446 cm^{-1}), v_6 (499 cm^{-1}) and v_5 (663 cm^{-1}) have been analyzed by Arié but only one hot subband can be found in the GEISA database. The sum of all the GEISA lines gives for v_5 an intensity of 108 $cm^{-2}\,atm^{-1}$ and 92.6 $cm^{-2}\,atm^{-1}$ for the fundamental band alone. Taking into account the partition function, we

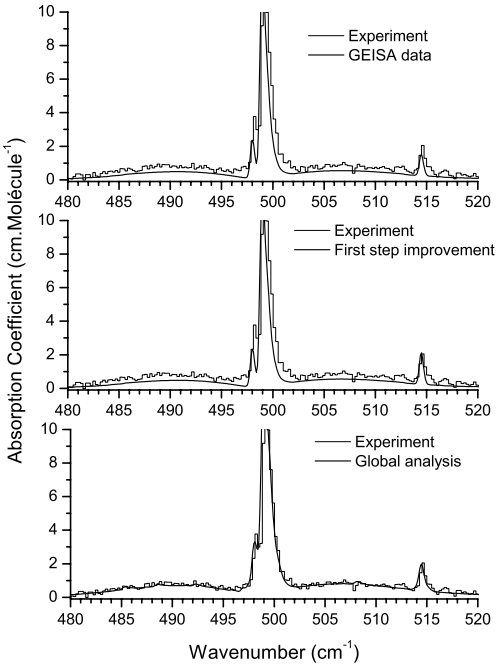

Fig. 5. Simulation of the v_6 band of HC_3N: comparison of our experimental spectrum at 0.5 cm^{-1} resolution with the calculated spectra using the data from GEISA (upper panel), the new improved parameters discussed in the text (middle panel) and the new line list from the global analysis (lower panel). The central Q branch has been truncated to help the comparison.

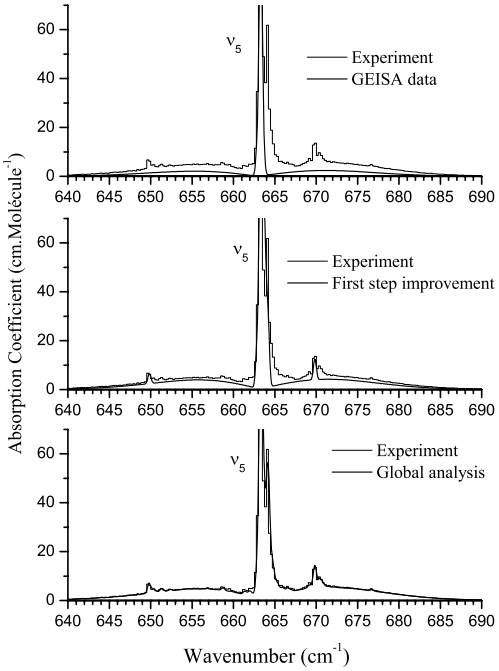

Fig. 6. Simulation of the v_5 band of HC_3N: comparison of our experimental spectrum at 0.5 cm^{-1} resolution with the calculated spectra using the data from GEISA (upper panel), the new improved parameters discussed in the text (middle panel) and the new line list from the global analysis (lower panel). The central Q branch has been truncated to help the comparison.

obtain a total band intensity of $92.6 * 3.02 = 279.6\ \mathrm{cm^{-2}\,atm^{-1}}$, a value which does not correspond to any of Khlifi's results but very close to Uyemura's result which might have been chosen in that case.

As can be seen in the upper panels of Figs. 5 and 6, the simulated spectra using the GEISA data cannot reproduce our experimental low resolution band spectra at room temperature. The total band intensity is largely underestimated because hot subbands with non-negligible intensities are not included in the database. The sum of the GEISA lines only accounts for 33% of the intensity of the v_5 band and 60% of the v_6 band.

For v_6 in HC_3N, two hot subband features assigned to the $v_6 + v_7(\Sigma^+) \leftarrow v_7(\Pi)$ and $2v_6(\Sigma^+) \leftarrow v_6(\Pi)$ subbands (Fig. 5 are clearly observed at 497.9 and 514.4 $\mathrm{cm^{-1}}$, respectively. The GEISA database underestimates the hot to cold band ratios in particular for the feature at 497.9 $\mathrm{cm^{-1}}$. For the v_5 band (Fig. 6), the discrepancy between the simulation and the experimental spectra is even more pronounced since very distinct hot subband features at 649.8 $\mathrm{cm^{-1}}$ ($2v_5(\Sigma^+) \leftarrow v_5\Pi$)) and 669.8 $\mathrm{cm^{-1}}$ ($2v_5(\Delta) \leftarrow v_5(\Pi)$) are missing in the model.

5. Hot band intensities

In order to improve the agreement between the calculated model spectra and our experimental low resolution spectra, we have, as a first step, included all the hot subbands analyzed by Arié which were missing in the GEISA data. For the v_5 band, all the twelve subbands analyzed by Arié [12] have been taken into account in this new simulation: four subbands belonging to $v_5 + v_7(\Sigma^+, \Sigma^-, \Delta) \leftarrow v_7(\Pi)$, three subbands belonging to $v_5 + 2v_7(\Pi, \Pi, \Phi) \leftarrow 2v_7(\Sigma^+, \Delta)$, three more belonging to $v_5 + v_6(\Sigma^+, \Sigma^-, \Delta) \leftarrow v_6(\Pi)$ and the two last subbands belonging to the $2v_5(\Sigma^+,\Delta) \leftarrow v_5(\Pi)$ group. For a few transitions, the assignment of the upper state was missing but plausible assignment could be found to include the transitions in the simulation. Unresolved subbands having the same band center such as the $2v_5(\Delta) \leftarrow v_5(\Pi)$ transition have been given a weight of two.

Another improvement in this first step progress concerns the hot to cold band intensity ratio. Rather few authors have considered the particular problem of the relative intensities of hot subband transitions [13–16]. All those experimental studies agree about the fact that, within a few percent, cold and hot bands have the same transition dipole moment. But according to the authors, a vibrational factor equivalent to the rotational Hönl-London factors, is to be taken into account. This numerical factor which is equal to one in the simplest cases, must be applied to each subband. The vibrational degeneracy of the bending modes is removed by ℓ-type interactions and each transition between the ℓ-substates Σ, Π or Δ are considered separately. Maki et al. [15] have obtained vibrational factors for many hot subbands in HCN and found values different from one for higher order overtone transitions. Both Weber's and Jacquemart's papers [14,16] deal with the v_5 bending mode of C_2H_2. The most interesting result of both papers concerning hot band intensities is that all subbands belonging to the transition $v_5 + v_4 \leftarrow v_4$ have a factor 0.5 while the group belonging to $2v_5 \leftarrow v_5$ have a factor of 1. Details about the calculation of those vibrational factors can be found in a paper [13] about hot band intensities in C_4N_2. On this basis, the vibrational factor for the intensity of the v_5 band and its associated hot subbands ($\Delta v_5 = +1$ transitions) of HC_3N comes from the square of the matrix element of the normal coordinate q_5:

$$|\langle v_5 + 1, \ell_5 \pm 1|q_5|v_5, \ell_5\rangle|^2 = \frac{v_5 \pm \ell_5 + 2}{2} \tag{4}$$

The vibrational factor depends on the v_5 and ℓ_5 quantum numbers of the lower state and on the sign of $\Delta\ell_5$. Furthermore, if the upper or the lower state of the transition (but not both) is a "full-zero" state (state with $\ell_5 = \ell_6 = \ell_7 = 0$), the intensity is multiplied by a factor 2. The calculation of the vibrational factors for all subbands of the v_5 complex illustrates the contributions from Eq. (4) (first factor) and from the eventual "full-zero" factor (second factor), with the notation $v_5\ v_6\ v_7$, $\ell_5\ell_6\ell_7$:

$v_5(\Pi) - \mathrm{g.s.}(\Sigma)$	$100, 100\text{–}000, 000$	$1 * 2 = 2$
$v_5 + v_7(\Sigma) - v_7(\Pi)$	$101, 10-1\text{–}001, 001$	$1 * 1 = 1$
$v_5 + v_7(\Delta) - v_7(\Pi)$	$101, 101\text{–}001, 001$	$1 * 1 = 1$
$v_5 + 2v_7(\Pi) - 2v_7(\Sigma)$	$102, 100\text{–}002, 000$	$1 * 2 = 2$
$v_5 + 2v_7(\Pi) - 2v_7(\Delta)$	$102, -102\text{–}002, 002$	$1 * 1 = 1$
$v_5 + 2v_7(\Phi) - 2v_7(\Delta)$	$102, 102\text{–}002, 002$	$1 * 1 = 1$
$v_5 + v_6(\Sigma) - v_6(\Pi)$	$110, 1-10\text{–}010, 010$	$1 * 1 = 1$
$v_5 + v_6(\Delta) - v_6(\Pi)$	$110, 110\text{–}010, 010$	$1 * 1 = 1$
$2v_5(\Sigma) - v_5(\Pi)$	$200, 000\text{–}100, 100$	$1 * 2 = 2$
$2v_5(\Delta) - v_5(\Pi)$	$200, 200\text{–}100, 100$	$2 * 1 = 2$

The vibrational factor is used as a relative intensity factor so that the value for the cold band is usually set to 1 and the factors for the hot subbands are equal to 0.5 or 1 in agreement with Jacquemart [14] and Weber [16].

We have to notice that the apparent intensity of the Q-branches in the low resolution spectra also depends on two points. First, the shape of the Q branch is a function of the ΔB value of the transition: some Q branches are quite sharp with a rotational structure concentrated on less than 0.1 $\mathrm{cm^{-1}}$, while some others are spread over about 1 $\mathrm{cm^{-1}}$. Second, we have a single Q branch for the Π–Σ and Σ–Π transitions while there are two Q branches with the same origin for other transitions (Δ–Π, Φ–Δ,...).

Including the correct vibrational factors and the 12 hot subbands mentioned above, we obtain a new simulated spectrum shown in the middle panel of Fig. 6. The simulation now accounts for about 80% of the total integrated intensity of the band. The hot subband features at 649.8 and 669.8 $\mathrm{cm^{-1}}$ are well reproduced by the model, but the double peak structure of the main band which is

accompanied by a feature at 664.2 cm^{-1} is not apparent in the simulation. The middle panel of Fig. 5 shows an improvement for the calculation of the v_6 band concerning the feature at 514.4 cm^{-1} which is now well reproduced, whereas the hot subband feature at 498.0 cm^{-1} and the general envelope of the band system are still underestimated.

Improvements in the fit of our experimental spectra are obvious compared to the GEISA data, but the integrated intensities and some hot subband features are still not perfectly reproduced. To reproduce our room temperature experimental spectra, it is clear that more hot subbands are to be introduced, but we have also to consider vibrational and rotational ℓ-type resonances and anharmonic resonances which could induce strong intensity perturbations, as shown in the recent study of C_4N_2 [13]. This has been possible thanks to the global rovibrational analysis programs developed in Louvain-la Neuve.

6. Global analysis

The goal of the global analysis is to fit simultaneously in a weighted least-squares procedure all data (microwave, mm-wave, RF, and infrared data) concerning the rovibrational energies in the electronic ground state of a given linear molecule. First developed for linear triatomic molecules [17], its principle has been applied successively to pentatomic [18,19], sexatomic [20], and tetratomic [21] linear molecules, and a detailed description is given about HCCNC in Ref. [19]. To reproduce the data within their experimental uncertainty, we have to develop a model with some off-diagonal terms: the vibrational and rotational ℓ-type resonances, and some anharmonic and Coriolis resonances if their effect is too strong or too local to be reproduced by perturbation methods. The model defined for HCCCN is explained in Ref. [19] where the Hamiltonian is also described, and complementary terms are given in the global analysis of $HCCC^{15}N$ [22]. For each polyad and for each J value of interest, we construct an energy matrix where all those off-diagonal terms of our Hamiltonian are taken into account simultaneously. The fit is done simultaneously on all available data on the basis of a set of molecular parameters which is progressively improved, and we can easily generate new predictions about the not yet assigned experimental data. Using the HC_3N spectra [12] kindly transmitted by Arié, we have been able to assign about 80 new hot subbands in the v_6, v_5, and $v_6 + v_7$ infrared bands (unpublished work). They concern higher energy states and most of them are heavily perturbed by various resonances. The quality of those data, combined with numerous new rotational transitions in the millimeter-wave range [18], yields a very good set of molecular parameters from which we reproduce roughly all observed states up to 2000 cm^{-1} in agreement with their experimental uncertainty (between 0.0001 and 0.001 cm^{-1}), and which allows good predictions (within 0.001–0.1 cm^{-1}) for the unobserved states.

Relative intensities are easily calculated for bands involving states free of any resonance, but most HC_3N states are perturbed by vibrational and/or rotational resonances. Those interactions perturb the corresponding energies but they also induce a mixing of the interacting states, mixing which is given by the coefficients of the eigenvectors which are determined in the global analysis. The general procedure we have developed to calculate relative intensities of linear molecule spectra is explained with details in a paper [13] about C_4N_2. This procedure is applied to the v_9 perpendicular band and its numerous hot bands in the same paper [13] and to the parallel $v_7 + v_9$ band in Ref. [20]. The important effects on intensities due to the vibrational and rotational resonances are illustrated by various examples. The same kinds of effects also appear in the HC_3N spectra, but furthermore anharmonic resonances (mainly the interaction between v_5 and $3v_7$) induce quite spectacular but more local intensity perturbations. We have checked line-by-line that those calculated intensity perturbations correspond within a few percent to the experimental high resolution spectrum of Arié et al. [12]. However, those general and local intensity perturbations will not stand out in the spectra recorded with a 0.5 cm^{-1} resolution, because the intensity exchanges occur between lines reaching states with the same J value and close to each other.

The calculation of spectra with intensities is fully automatic. We define the maximum energy we have to consider for the lower states (for v_5: 1522 cm^{-1}, what corresponds to the 123 substates belonging to the first seven polyads) and the transition moment associated with the selection rule (for v_5: $\Delta v_5 = +1$) which defines the upper polyads to be considered. All lines with intensity above some threshold are considered in the calculated spectrum.

A list of lines with their position and relative intensities have been generated for the v_5 and v_6 complexes. The integrated band intensities measured in this work have been used to obtain the absolute intensity for each line.

Using this new line list, we obtain a very good fit for our low resolution experimental spectra as can be seen in the lower panels of Figs. 5 and 6. The main result from the global analysis is that enough hot subbands are taken into account so that the overall integrated intensity of the bands is perfectly reproduced. Moreover, the discrepancies concerning the hot subband features which remained after the first step improvement have now vanished. In the v_6 band, we have solved the problem at 498.0 cm^{-1}. The progress comes from including three new hot subbands from the $v_5 + 2v_7 \leftarrow 2v_7$ group of transitions with band centers close to 498.0 cm^{-1}. They add their intensities to the $v_6 + v_7(\Sigma^+) \leftarrow v_7(\Pi)$ Q branch to produce the strong feature observed at this wavenumber. For v_5, the strong feature at 664.2 cm^{-1} is now well reproduced by the model. It is mainly assigned to $v_5 + v_7(\Sigma^+) \leftarrow v_7(\Pi)$ at 664.151 cm^{-1} but also to two other hot subbands

($\nu_5 + 2\nu_7(\Pi,\Phi) \leftarrow 2\nu_7(\Delta)$) with band centers at 664.227 and 664.255 cm^{-1}. We have also to notice that the subbands with code P, Q, T, and V in Ref. [12] are at least partly misassigned.

In Fig. 7 we zoom on the ν_5 room temperature low resolution spectrum to illustrate the contribution of the successive groups of hot subbands that we consider in the new line list for ν_5 (see figure caption for details). We will first make general comments about those hot subbands, and after we will have a look to special features in the spectrum.

Going from one curve to the next one, from (a) to (+g), we increase by one unit the vibrational quantum number ν_7, what roughly corresponds to an increase of 222 cm^{-1} in energy, and so to a reduction of the lower state population by a factor 3.0 according to the Boltzman law. However, the decrease of the contribution of the groups of hot subbands according to ν_7 is not so dramatic because both upper and lower polyads contain more and more substates, and so the number of hot subbands rapidly increases. As an example, if the group from the ν_7 state contains 7 hot subbands, the group from the $3\nu_7$ polyad contains 60 hot subbands. Furthermore, when ν_5 in the lower state is different from zero, the vibrational factor enhances the intensity. For those reasons, to explain all observed Q branches and to make negligible the contribution of the non-included hot subbands, we had to consider more than 500 hot subbands, up to the group starting from the $6\nu_7$ polyad, what corresponds to lower states up to 1520 cm^{-1}.

About the hot subband Q branches in Fig. 7, we have to keep in mind that many of them are hidden by stronger ones, particularly between 663 and 665 cm^{-1}. In the third curve, where the (c) contribution appears, the Q branches at 661.3 and 666.5 cm^{-1} are assigned to the ($\nu_5 + 2\nu_7 \leftarrow 2\nu_7$) $\Pi \leftarrow \Delta$ and $\Pi \leftarrow \Sigma$ transitions, respectively. The strongest Q branches from the (d) contribution are observed at 649.8 and 669.8 cm^{-1} and are assigned to the $(2\nu_5 \leftarrow \nu_5)\Sigma \leftarrow \Pi$ and $\Delta \leftarrow \Pi$ transitions, respectively. As explained previously their intensity is enhanced by a favorable vibrational factor, but the second one is twice as strong as the first one because there are two superposed Q branches, the $\Delta^e \leftarrow \Pi^f$ and $\Delta^f \leftarrow \Pi^e$ transitions. Hot subband features from even higher energy states can be identified, for instance the (e) contribution to the spectrum at 650.5, 651.4, 669.1, and 670.3 cm^{-1}, which are assigned to the $2\nu_5 + \nu_7 \leftarrow \nu_5 + \nu_7$ transition. An example of the (f) contribution, the $2\nu_5 + 2\nu_7 \leftarrow \nu_5 + 2\nu_7\Sigma^e \leftarrow \Pi^f$ transition can be distinguished at 652.4 cm^{-1}. The strongest Q branches from the (g) group correspond to hot subbands from $2\nu_5$, enhanced by the vibrational factor and their superposition:

$3\nu_5(\Pi) - 2\nu_5(\Sigma)$	300, 100–200, 000	$2 * 2 = 4$	*f–e*
$3\nu_5(\Pi) - 2\nu_5(\Delta)$	300, 100–200, 200	$1 * 1 = 1$	*f–e* and *e–f*
$3\nu_5(\Phi) - 2\nu_5(\Delta)$	300, 300–200, 200	$3 * 1 = 3$	*f–e* and *e–f*

They appear at 656.83, 636.85, and 676.71 cm^{-1}, respectively. The lower states lie at 1313 (Σ) and 1333 (Δ) cm^{-1}. Finally, the (h) contribution, from the ^{13}C and ^{15}N isotopologues, is overlapped by the strong central Q branch, except for $H^{13}CCCN$ of which the cold band Q branch is observed at 658.7 cm^{-1}.

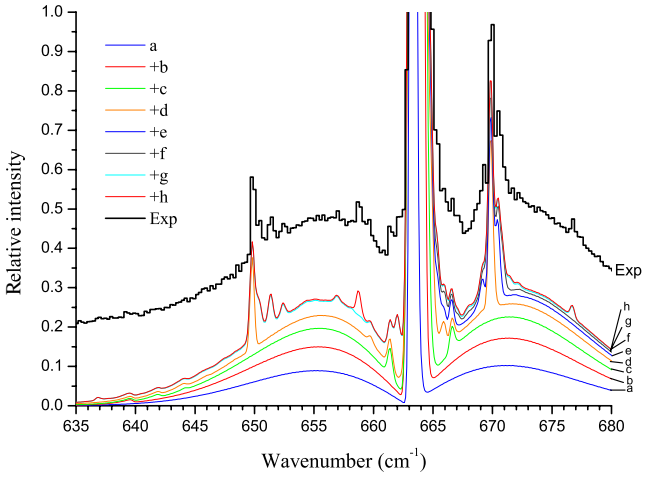

Fig. 7. Progressive addition of the groups of hot subbands in the ν_5 low resolution spectrum of HC_3N: (a) cold band, (b) hot subbands from ν_7, (c) hot subbands from the polyad ($2\nu_7$, ν_6), (d) from the polyad ($3\nu_7$, ν_5, $\nu_6 + \nu_7$), (e) from the polyad ($4\nu_7$, $\nu_5 + \nu_7$, ν_4, $\nu_6 + 2\nu_7$, $2\nu_6$), (f) from the polyad ($5\nu_7$, $\nu_5 + 2\nu_7$, $\nu_4 + \nu_7$, $\nu_5 + \nu_6$, $\nu_6 + 3\nu_7$, $2\nu_6 + \nu_7$), (g) from the polyad ($6\nu_7$, $\nu_5 + 3\nu_7$, $2\nu_5$, $\nu_4 + 2\nu_7$, $\nu_4 + \nu_6$, $\nu_5 + \nu_6 + \nu_7$, $\nu_6 + 4\nu_7$, $2\nu_6 + 2\nu_7$, $3\nu_6$), (h) the cold band and the hot subbands from ν_7 of the main ^{13}C and ^{15}N isotopologues. The experimental spectrum has been shifted up by 0.2 to help the comparison and the central Q branch has been truncated to help the comparison.

7. Application to Titan

On Titan, the hot band problem is largely simplified since the temperature range sounded by infrared spectroscopy on Titan is low, between 150 and 200 K. However, the population in the ground state of HC_3N at 200 K is no more than 59%, what means that 41% of the integrated intensity comes from the hot subbands. According to the latest infrared observation of Titan [3], the abundance of HC_3N increases above 60° north in latitude and reaches a maximum at the north pole with a volume mixing ratio of 6×10^{-8}. The temperature increases also towards the north pole to reach 200 K. Using our new line list we have calculated the shape of the HC_3N ν_5 band (Fig. 8) at a temperature of 200 K and a resolution of 0.5 cm^{-1}, the resolving power of the infrared spectrometer (CIRS) of the Cassini spacecraft. A simulation done with the GEISA line list is also shown. The hot subband feature at 664.2 cm^{-1} is still strong since it is only 4-times weaker than the main band. The Q branches of the hot subbands from ν_5 are still visible at 649.8 and 669.8 cm^{-1}. The Q branch at 658.7 cm^{-1} is associated with the cold band of $H^{13}CCCN$. The shoulder at 664.2 cm^{-1} should be easily observed with CIRS and the modeling of HC_3N on Titan should be largely improved.

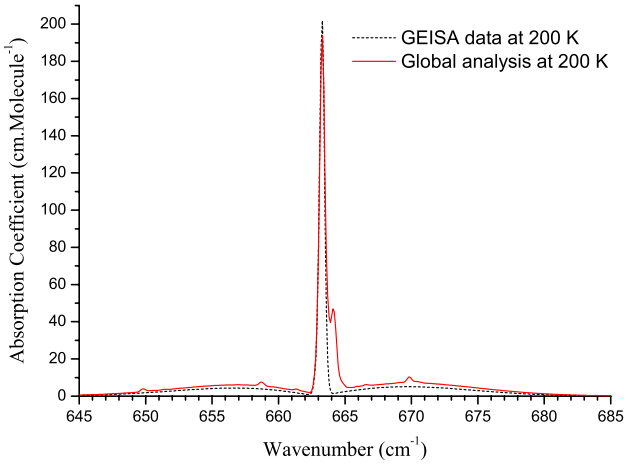

Fig. 8. Simulated spectra of the ν_5 band of HC_3N at 200 K using the GEISA line list and the line list derived from the global analysis.

8. Conclusion

In this new experimental work on HC_3N band intensities, we have obtained a good agreement with the previous results by Uyemura. Exploring the linear and the saturation zones of absorption spectra we have shown that some former results by Khlifi were obtained under non-linear conditions. Accordingly, we recommend using the integrated band intensities obtained in this work and consider a 5% confidence margin. Concerning the temperature dependence, we recommend using the $1/T$ expected variation of the integrated band intensities since we have shown that Khlifi's results do not disprove it.

Our experimental spectra at 0.5 cm^{-1} resolution could be compared to calculated spectra which were obtained by using the line list from the GEISA database. Large discrepancies concerning the integrated band intensities and the hot subband features have appeared due to the lack of non-negligible hot subbands. We have shown that the fit can be improved by taking into account a larger number of subbands and by calculating the vibrational factors in a rigorous manner. However, a very good fit can only be obtained on the basis of the global analysis. A new line list, available on request to the corresponding author of this paper, is obtained from this work combining the measured integrated intensity and the new analysis. Any spectra can be calculated from this line list at various temperature and instrumental resolution. Applied to Titan, we have calculated a spectrum at 0.5 cm^{-1} resolution and 200 K, and we have shown that hot subband Q branches should be detected for HC_3N on Titan.

References

[1] V.G. Kunde, A.C. Aikin, R.A. Hanel, D.E. Jennings, W.C. Maguire, R.E. Samuelson, Nature 292 (1981) 686–688.
[2] A. Coustenis, B. Schulz, S. Ott, E. Lellouch, T. Encrenaz, D. Gautier, H. Feuctgruber, Icarus 161 (2003) 383–403.
[3] N.A. Teanby et al., Icarus 181 (2006) 243–255.
[4] J. Cernicharo, A.M. Heras, J. Pardo, A. Tielens, M. Guelin, E. Dartois, R. Neri, L. Waters, Astrophys. J. 546 (2001) 127–130.
[5] M. Uyemura, S. Maeda, Bull. Chem. Soc. Japan 47 (1974) 2930–2935.
[6] M. Uyemura, S. Degushi, Y. Nakada, T. Onaka, Bull. Chem. Soc. Jpn. 55 (1982) 384–388.
[7] M. Khlifi, F. Raulin, E. Arié, G. Graner, J. Mol. Spectrosc. 143 (1990) 209–211.
[8] M. Khlifi, F. Raulin, M. Dang-Nhu, J. Mol. Spectrosc. 155 (1992) 77–83.
[9] K.M.T. Yamada, H. Bürger, Z. Naturforsch. A 41 (1986) 1021–1023.
[10] R.A. Creswell, G. Winewisser, M.C.L. Gerry, J. Mol. Spectrosc. 65 (1977) 420–429.
[11] K.M.T. Yamada, R.A. Creswell, J. Mol. Spectrosc. 116 (1986) 384–405.
[12] E. Arié, M. Dang Nhu, Ph. Arcas, G. Graner, H. Bürger, G. Pawelke, M. Khlifi, F. Raulin, J. Mol. Spectrosc. 143 (1990) 318–326.
[13] A. Fayt, C. Vigouroux, F. Winther, J. Mol. Spectrosc. 224 (2004) 114–130.
[14] D. Jacquemart, C. Claveau, J.-Y. Mandin, V. Dana, JQSRT 69 (2001) 81–101.
[15] A.G. Maki, W. Quapp, S. Klee, J. Mol. Spectrosc. 171 (1995) 420–434.
[16] M. Weber, W.E. Blass, G. Halsey, J. Hillman, J. Mol. Spectrosc. 165 (1994) 107–123.
[17] A. Fayt, R. Vandenhaute, J.G. Lahaye, J. Mol. Spectrosc. 119 (1986) 233–266.
[18] L. Mbosei, A. Fayt, P. Dréan, J. Cosléou, J. Mol. Struct. 517–518 (2000) 271–299.
[19] C. Vigouroux, A. Fayt, A. Guarnieri, A. Huckauf, H. Bürger, D. Lentz, D. Preugschat, J. Mol. Spectrosc. 202 (2000) 1–18.
[20] F. Winther, V.-M. Horneman, C. Vigouroux, A. Fayt, J. Mol. Struct. 742 (2005) 131–146.
[21] S. Robert, M. Herman, J. Vander Auwera, G. Di Lonardo, L. Fusina, G. Blanquet, M. Lepère, A. Fayt, Mol. Phys., in press.
[22] A. Fayt, C. Vigouroux, F. Willaert, L. Margules, L.F. Constantin, J. Demaison, G. Pawelke, El B. Mkadmi, H. Bürger, J. Mol. Struct. 695–696 (2004) 295–311.